Eurographics Workshop on Visual Computing for Biology and Medicine (2019)
K. Lawonn and R. G. Raidou (Editors)

Short Paper

Layer-Aware iOCT Volume Rendering for Retinal Surgery

J. Weiss[1] U. Eck[1] M. A. Nasseri[2] M. Maier MD[2] A. Eslami[3] N. Navab[1,4]

[1]Technical University Munich, Germany
[2]Dep. of Ophthalmology, Klinikum rechts der Isar, TUM, Germany
[3]Carl Zeiss Meditec, Munich, Germany
[4]Johns Hopkins University, Baltimore, USA

Abstract

Retinal microsurgery is one of the most challenging types of surgery, yet in practice, intraoperative digital assistance is rare. The introduction of fast, microscope integrated Optical Coherence Tomography (iOCT) has enabled intraoperative imaging of subsurface structures. However, effective intraoperative visualization of this data poses a challenging problem both in terms of performance and engineering as well as for creating easily interpretable visualizations of this data. Most existing research focuses on visualization of diagnostic OCT data where imaging quality is higher and processing times are not an issue. We introduce a perceptually linear color map for a separated encoding of tissue reflectivity and positional information as chrominance and luminance. Based on this color mapping, we propose a Direct Volume Rendering (DVR) method that aids structure perception. To aid subretinal injection tasks, we introduce a novel Layer-Adjusted Maximum Intensity Projection (LA-MIP), correcting for the natural curvature of the retinal tissue. Expert feedback suggests our methods are preferred over baseline methods. Further research is needed to confirm the benefits of our approach in routine clinical applications.

CCS Concepts

• ***Human-centered computing*** → ***Scientific visualization;*** • ***Computing methodologies*** → *Perception;*

1. Introduction

In posterior ophthalmic microsurgery, the structures that have to be manipulated are on the scale of microns. Manual manipulation with forceps and other tools mean that the precision at which instruments have to be guided with a precision that is close to natural hand tremor. The surgical scene can only be observed through a microscope looking through the patient's lens and pupil, making any additional intraoperative help or guidance for the surgeon is highly valuable. OCT, an imaging modality widely used in diagnosis and progression monitoring in the ophthalmic clinic, has been introduced into surgical microscopes, with a first commercially available device in 2014.

OCT is a tissue imaging modality that measures the light reflected from different tissue depths, with characteristics similar to ultrasound. Carrasco-Zevallos et. al [CZVK*17] provide a thorough overview on existing systems for intraoperative OCT (iOCT) as well as their applications. Most of these systems, however, are at a research prototype stage only. While state-of-the-art iOCT systems reach and surpass A-Scan rates of 1MHz and resolutions as low as 1μm [CZKV*16, KDK*19], current commercially available iOCT systems have an A-Scan rate of 27-35 kHz, resulting in acquisition times of 1-2 seconds for a volume. While this is not suitable for real-time volumetric feedback, it enables a workflow where the surgeon pauses for the imaging to assess the surgical situation in a 3D view. At the time of writing, however, these devices do not include any advanced intraoperative visualization of that volumetric data. Among other procedures, iOCT has been shown to be beneficial in ERM peeling procedures [EKP*17], a procedure that requires the removal of a thin membrane attached to the retinal surface. With the recent introduction of precise ophthalmic robotic surgery systems [REG18], 3D visual guidance of robotic maneuvers during operations like subretinal injections becomes much more important.

This manuscript focuses on visualization techniques for volumetric intraoperative OCT data in retinal microsurgery. In this paper we first provide a short analysis of the state of the art which motivates the development of our own ideas. We then introduce a class of perceptually linear color maps to aid structural understanding (subsection 3.1). We use this color map in a DVR approach that enhances spatial understanding of superficial details as well as layer thickness variations (subsection 3.2). We further propose a Layer-Adjusted Maximum Intensity Projection (LA-MIP) to help perceive whether the instrument is close to or below the retinal surface (subsection 3.3). We show results on exemplary cases section 4 and report initial feedback from two expert surgeons. We discuss the limitations of the proposed methods and highlight further research needed in this application area (section 5) before concluding with a short summary.

DOI: 10.2312/vcbm.20191239

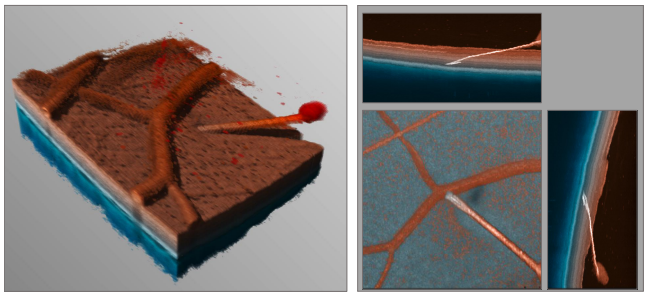

Figure 1: *Local shadowing together with a colorization relative to an anatomical reference layer provides clear visualization of epiretinal structures (left). A colorized en-face projection combined with a novel layer-adjusted MIP provides improved visualization of instrument position below the surface (right).*

2. Related Work

With iOCT as a generic 3D volumetric data cube, all generic direct volume rendering approaches can be applied [ZEP11, SSN*98, BG09], however they are, for the most part, unable to provide sufficient visualization of internal structures. In the current clinical practice, slice-based review of the data cube is the most common way surgeons interact with the volumetric data. In diagnostic systems OCT cubes are often reviewed via en face projections of slabs, where each pixel corresponds to the averaged intensities of an A-Scan between two tissue boundaries. Until recently, intraoperative volumetric OCT has been presented either on a secondary external screen, or through the use of monocular or stereoscopic screens integrated into the microscope [CZKV*16]. In research setups, feedback of 3D visualization has shown promise and are seen as the way forward [EUS18]. Viehland et al. [VKCZ*16] have developed a volume rendering method method specific to OCT volumes. They combine classic Phong-shaded Direct Volume Rendering (DVR) with enhancements for samples with high gradient magnitude, voxels with gradient perpendicular to the viewing direction as well as adding a slight colorization with increasing depth. They demonstrate improved perception of structures in OCT volumes. Bleicher et al. extend this approach with axial colorization of intraoperative OCT volumes [BJAV*18]. In their work, they apply colorization of the OCT based on the axial position relative to a re-computed center of mass. To our knowledge, the only rendering methods that are specifically proposed for OCT is by Viehland et al. [VKCZ*16] and its extension to axial colorization by Bleicher et al. [BJAV*18]. This method has been impact-full and is already used in several studies ([CZKV*16, KDK*19], among others). This led us to evaluate it in the context of our two use cases. In own experiments with different data sets, we have found their approach to be especially susceptible to noise. Viehland et al. mitigate this problem by applying a 3D Gaussian filter to remove much of the noise. However, this also has the effect of reducing visibility of the small structures we are interested in. In our own attempts to visualize data sets with their method with a lower amount of denoising, a good visualization could often only be found by turning off the gradient enhancement, and even then slight changes to the transfer function limits could have a high negative impact. The depth enhanced colorization method introduced in [BJAV*18] has shown promising results for iOCT rendering by increasing the visual contrast and adding depth cues through colorization. However, their approach uses a fixed axial reference position for the colorization to enhance tissues at different depths. According to discussions with our clinical experts, differences in absolute depth position are not always of direct interest. Natural curvature of the retina leads to color differences which have to be differentiated from actual structural anomalies. Lastly, the method was specifically designed to provide enhanced visualization of superficial structures. However, in the case of subretinal injections, an accurate visualization of spatial relations below the retinal surface is needed.

3. Layer-Aware Rendering of intraoperative OCT

An important reference is the Retinal Pigment Epithelium (RPE) layer, a hyper-reflective layer below the retinal surface: in ERM peeling, distance from this layer is a reliable factor for structural analysis while in subretinal injections, RPE is the most important boundary that should not be punctured yet approached as closely as possible. We present a volumetric rendering concept that aids understanding of superficial retinal structures. It highlights small superficial structures through a combination of enhancement methods, making it well-suited for ERM peeling and other surgeries where good perception of the surface is important. We supplement this with a *Layer-Adjusted Maximum Intensity Projection* (LA-MIP) which extends axis-aligned maximum intensity projections of OCT data and allows for a better assessment of needle penetration depth during an injection.

3.1. Perceptually Linear Depth Encoding Color Maps

Perception of depth differences is a major concern for both use cases: In ERM peeling, subtle surface irregularities are important to understand while for subretinal injection, the precise needle penetration depth and distance from the target layer are crucial.
We designed a color mapping function that can map two values, axial position and OCT intensity, to a color value. To ensure good visual separation of these two parameters, we map them to different perceptual parameters: Luminance and chrominance. This is important to allow surgeons to retain structural perception of the OCT intensity while adding additional information about depth, creating more visual contrast between different positions.
We assume the existence of an RPE layer map $\mathrm{rpe} : p \mapsto [0,1]$ giving the axial position of the RPE layer corresponding to the A-Scan containing position p. To ensure that linear changes in the parameters are also perceived linearly, we make use of the L*a*b* color space, which is designed to be perceptually linear [TT03]. To map each voxel p to a color, we first define a *depth predicate* $\delta(p) \in \mathbb{R}$ which encodes the depth of a voxel relative to the RPE reference layer as $\delta(p) = (p_x - \mathrm{rpe}(p))/d_{\mathrm{rpe}}$ where d_{rpe} is a normalization factor which is chosen to match the average thickness of the whole retinal tissue. To limit the colorization effect to differences close to the retinal tissue, we define a normalized version as $\delta^*(p) \in [-1,2]$ as $\delta^*(p) = \mathrm{clamp}_{[0,1]}((\delta(p)+1)/3)$. With this normalized predicate, we then define the color mapping function as an interpolation between two points $C_0 = (I(p), a_0, b_0), C_1 = (I(p), a_1, b_1)$ on the plane $L = I(p)$, as visualized in Figure 2:

$$C_{L^*a^*b^*}(I,\delta^*) = \gamma(I) \cdot \left(\delta^* \cdot C_1 + (1-\delta^*) \cdot C_0\right) \qquad (1)$$

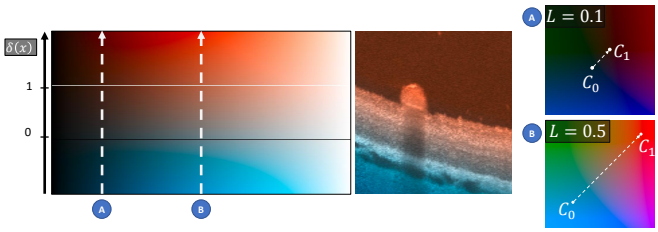

Figure 2: *Resulting color map for $C_0(L) = (L, -0.5, -0.5)$ and $C_1(L) = (L, 0.75, 0.75)$: $I(p)$ increases towards the right, Y axis shows changing values of $\delta(p)$. The effect of the scaling function $\gamma(I)$ is equivalent to moving the two points closer to $(0,0)$ in the a^*b^* plane for intensity I close to 0 or 1.*

We introduce the scaling factor $\gamma(I) = 1 - (I - 0.5)^2$ which is a parabola with a maximum at $\gamma(0.5) = 1$ and $\gamma(0) = \gamma(1) = 0$. This reduces the saturation of the colors for very high and very low image intensity values $I(p)$ and keeps the color values within the visible color gamut. With this framework, we can define a class of color maps on the a^*b^* plane defined by the two points C_0, C_1. For our visualizations, we fix $C_0(L) = (L, -0.5, -0.5)$ and $C_1(L) = (L, 0.75, 0.75)$ as this gives us a color gradient from blue to red (see Figure 2),

3.2. DVR for ERM Peeling

We have designed a volume rendering method that provides enhanced perception of superficial features and is based on the standard GPU volume raycasting pipeline [KW04]. We combine our color mapping with a linear opacity transfer function. Because our depth predicate δ is based on the distance to the closest RPE position, global curvature does not have an effect on our colorization. We avoid gradient-based shading by using shadow rays as discussed in [RKH08]. This straightforward way to implement volume shadows casts a shadow ray from every sample towards the light direction, sampling the intensities to accumulate a shadowing factor. This not only avoids dependency on a noisy gradient but additionally creates more visual fidelity by adding shadows, which has been shown to improve structural perception [DRN*17]. We also test a variant where the number of steps N_s a shadow ray takes is fixed. This not only limits the performance impact on the rendering but also shortens the distance across which shadows are cast. Contrary to Viehland et al. [VKCZ*16], we do not use any elaborate opacity boosting but apply a color transfer function computed on the fly for every raymarch sample. Our opacity transfer function $\alpha(I)$ is a piece-wise linear transfer function with range $[I_{min}, I_{max}]$ based on intensity only. We compute the final RGB color and opacity for a sample position as

$$C(p) = \left[s(p) \cdot \mathrm{RGB}\left(C_{L^*a^*b^*}\left(I(p), \delta^*(p)\right)\right), \alpha(I(p))\right] \quad (2)$$

where $RGB(C)$ is an $L^*a^*b^*$ to RGB color space conversion and $s(p)$ is the shadow factor determined as

$$s(p) = \prod_{0 \cdots N_s}^{i} \left(1 - \alpha(I(p + i \cdot L(p)))\right) \quad (3)$$

with $L(p) = |p_{Light} - p|$ and p_{Light} is the virtual light source position.

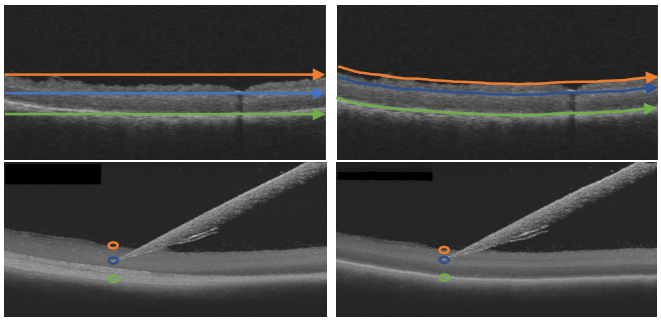

Figure 3: *Schematic view of our layer-adjusted MIP projection: Instead of projecting along straight, axis-aligned rays (left), we propose a projection along curved lines adjusted to the profile of the reference layer (right). This leads to better visualization of the actual distance between instrument and target layer.*

3.3. Layer-Adjusted MIP Projection

In subretinal injection, the needle needs to be placed as close to the hyper-reflective RPE layer as possible while avoiding puncture. While maximum intensity projections have shown good visualization as the maximal intensity corresponds to important pixels such as the needle or the RPE layer, these objects suffer from poor visibility when applied to an iOCT volume directly: Due to the natural curvature of the retinal surface, the target layer is not easily recognizable. We propose a *layer-adjusted MIP* (LA-MIP) which instead of projecting along straight lines through the volume, projects along lines that are parallel to the reference RPE layer. Effectively, this produces an image where every pixel corresponds to the projection along a curve that has a constant axial distance to the reference layer. Figure 3 illustrates the basic idea. To compute an output pixel color for a screen space pixel at normalized position $P = (P_x, P_y) \in [0,1]x[0,1]$, we set up the projection start and direction as $p_0 = (P_x, P_y, 0), d = (0,0,1)$. The reference layer distance for one ray is then $\delta_{ref}(P) = p_y - \mathrm{rpe}(p_0 + 0.5 * d)$. When marching through the volume, the original sampling position is $p_i = p_0 + \frac{i}{N-1} \cdot d$ for a sample with index i out of N total samples. We adapt the sampled X position to have the same distance to the sample's RPE layer height:

$$p_i^*(P) = \left(\mathrm{rpe}(p_i) + \delta_{ref}(P), p_{i,y}, p_{i,z}\right)^T \quad (4)$$

To compose the final color, we apply our distance encoding transfer function using the depth predicate from the reference layer:

$$C_{\mathrm{LAMIP}}(P) = C_{L^*a^*b^*}\left(\max_{i \in [0 \ldots N-1]} \{p_i^*(P)\}, \delta^*(p_0 + 0.5 \cdot d)\right) \quad (5)$$

We generate a projection in the y direction analogously by permuting the coordinates accordingly and combine these two views with an en face projection (see Figure 5), where every pixel is colored according to our color map using the maximal intensity and its respective location for colorization.

4. Results

To provide the reference RPE layer, we use the segmentation algorithm of the Cirrus HD (Carl Zeiss AG, Germany) diagnostic

OCT device and import the results for our iOCT volumes into our rendering framework. To reduce the speckle noise apparent in our iOCT cubes while keeping small structures, we apply a 3x3 median filter on every B-Scan but do not perform the volumetric Gaussian smoothing suggested in [VKCZ*16]. We implemented both our visualizations using C++ and OpenGL as fragment shader programs. The shadowing factor is computed per sample on the fly without caching. For the limited length shadows, we set $N_s = 20$ to provide real time performance with small local shadows. For the full shadowing, the shadow rays are terminated a maximum of $N_s = 200$. For simplicity of implementation, we do not employ acceleration structures except for early ray termination when ray opacity $\alpha > 0.975$. For our visual comparisons, we also implemented the raymarching of [VKCZ*16] inside our own framework to ensure our benchmarking is comparable. Visualization parameters and transfer function were manually adapted to achieve good visibility for our OCT characteristics. All OCT scans used were acquired from a Carl Zeiss Lumera 700 operating microscope with a RESCAN 700 integrated OCT [Zei]. For each OCT data set we manually selected a transfer function intensity range I_{min}, I_{max} that was used for all renderings of the same data set. All our tests were performed on a machine with an Intel i7 8700K CPU and an NVidia Titan Xp GPU. We measured an average total of 1.6s for segmentation and 0.3s for volume median filtering. We benchmarked the raymarching methods by measuring average frame time for rendering a 512x512x128 volume at a resolution of 1024x1024 during one full rotation (360 frames) of the volume around the Z axis. The baseline methods [VKCZ*16, BJAV*18] achieve 4.6ms and 5.6ms. Our colorized raymarching requires 4.5ms without any shading, 8.6ms for $N_s = 20$ shadow steps and 31.1ms for $N_s = 200$. The composed LA-MIP projection view consisting of all three projections is generated in 1.1ms.

Example Cases. We have selected several iOCT volumes to highlight the results when applying the different variants of iOCT visualization. Figure 4 shows a case after ERM peeling. The macular hole can be seen at the center of the images. The peeled ERM is positioned above the macular hole as an *inverted flap*, which has been shown to improve healing. 3D iOCT is especially helpful in this case to check whether its placement over the hole is correct. The different shading options applied here illustrate that without any shading or with gradient-based shading, perception of the relative positioning is challenging. The variants using shadow rays produce a softer appearance and the additional shadows help understanding the 3D relationship. Our DVR method is able to provide better visualization of smaller superficial structure when compared to the baseline method. Figure 1 demonstrates a needle at the ideal positioning for injection in an ex-vivo porcine eye. With our composite view of an en face view and two LA-MIP views, the needle position can be easily assessed in all three directions. Figure 5 exemplifies a situation where the surgical instrument touches the retinal surface. From the DVR rendered view, deformations of the surface can be monitored while the LA-MIP views allow for a better assessment of the needle tip position.

Expert Feedback. We have presented several cases of iOCT acquired during routine epiretinal surgery to two expert ophthalmic surgeons with clinical experience of 27 and 12 years, respectively. Both stated that they work with iOCT regularly, although none of them have used a system that shows 3D cubes intraoperatively in a clinical setting. In our interview session, we presented several variations of visual parameters (rotation speed, inclination, aspect ratio, illumination model and colorization scheme) on a total of 8 different data sets in order to find sensible default values for an automated, interaction-free visualization. The interviewed surgeons suggest a rotation speed of about 45deg/s and an inclination angle of about 25deg with respect to the retinal tissue should work well for the presented cases. Comparing the shading options, our surgeons preferred shadow rays for all cases, judging it to be more natural and intuitive compared to Phong shading. Notably, in two cases with layer-relative colorization, the un-shaded option was judged to be of similar value as the other versions are significantly darkened. The two expert surgeons stated that limited shadow rays provide higher value due to their smaller occlusion radius. Colorization options were appreciated more when a depth-based colorization was applied than with axial colorization. Ideally, unique color should map directly to specific retinal layers, which is close to our approach at least for non-pathological cases. Nonetheless, one surgeon remarked that intensity-based transfer functions with a high number of color bands seem to be better at enhancing the high reflectivity of the RPE layer, demarcating it as a clear line which is sometimes desirable.

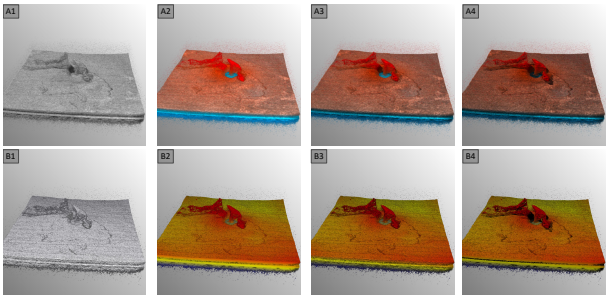

Figure 4: *Retinal flap positioning to close the hole with different shading options.* ***A1:*** *Local Shadow Rays only,* ***A2:*** *Depth-based Colorization only,* ***A3:*** *Limited Shadow Rays,* ***A4:*** *Full Shadow Rays* ***B1:*** *Shading and opacity enhancement [VKCZ*16],* ***B2:*** *Axial colorization and opacity enhancement (no Phong shading),* ***B3:*** *Visualization as in [BJAV*18].* ***B4:*** *Same as* ***B3*** *but with shadow rays instead of Phong shading.*

5. Discussion and Conclusion

The visualization concepts we have proposed both rely on a segmentation of an anatomical layer that can be used as a reference. In our experiments we used an existing implementation that was not optimized for iOCT volumes and thus sometimes exhibited areas of faulty segmentation, especially in the presence of instruments. An incorrect segmentation map can strongly influence the quality of the visualization, potentially leading to distorted projections and confusing colorization. We are positive that with a properly adapted algorithm specialized for single-layer segmentation of intraoperative volumes, this can be sufficiently solved to reduce the occurrence of segmentation artifacts.
We have gathered initial subjective feedback from two surgeons which indicates a preference towards our proposed method. While

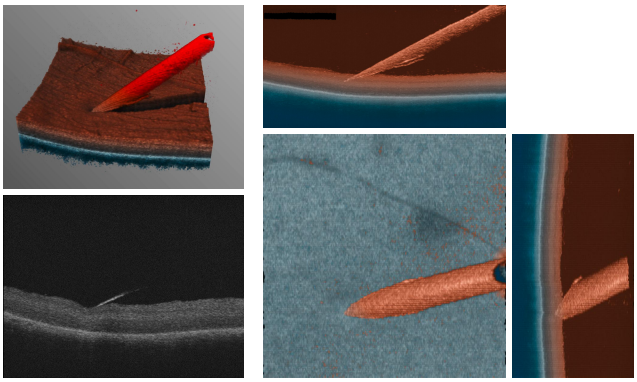

Figure 5: *Needle touching the retinal surface. From DVR it is not directly apparent whether the needle has already perforated while B-Scan inspection suffers from misalignment, making the information unreliable. Our final composed image of en face and LA-MIP views show clearly that the needle is below the surface, but far enough from the RPE layer.*

this is not representative, it gives important direction and motivates further investigation to assess the clinical benefit of our proposed method. A more structured and objective validation needs to be performed, including a larger user group preferably consisting of clinical experts and a measurable task that can objectively assess the efficacy of our visualizations.

We have shown two visualization methods for advanced intraoperative feedback, based on the idea of distance-based colorization with respect to an anatomical layer. To support this, we developed a color mapping that encodes both intensity and depth in a perceptually linear way to ensure good perception of both dimensions separately. Expert surgeon feedback indicates that our concepts are worth investigating further as a promising way towards more visually appealing and intuitively helpful intrasurgical feedback. In future extensions of this work we would like to formally evaluate the benefit of our method as well as tackle remaining stepping stones such as a real-time approximate RPE segmentation to work towards a seamless integration into the surgical workflow.
While our first results look promising, this only provides one step towards exploring more advanced rendering and visualization methods for iOCT. OCT in general and iOCT specifically provides many further interesting challenges in both rendering and visualization: 4D capable engines introduce hard real time constraints to process the acquired data on time, while on the other end novel display devices like stereo displays, virtual and augmented reality headsets increase the required rendering resolution and framerate requirements even higher.

Acknowledgements We thank NVIDIA Corporation for the donation of the Titan Xp used in our experiments. This research has been partially funded by the Federal Ministry of Education and Research of Germany (BMBF) in the framework of Software Campus 2.0 (FKZ 01IS17049).

References

[BG09] BRUCKNER S., GRÖLLER M. E.: Instant Volume Visualization using Maximum Intensity Difference Accumulation. *Computer Graphics Forum 28*, 3 (2009), 775–782. 2

[BJAV*18] BLEICHER I. D., JACKSON-ATOGI M., VIEHLAND C., GABR H., IZATT J. A., TOTH C. A.: Depth-Based, Motion-Stabilized Colorization of Microscope-Integrated Optical Coherence Tomography Volumes for Microscope-Independent Microsurgery. *Transl. Vis. Sci. Technol. 7*, 6 (nov 2018), 1. 2, 4

[CZKV*16] CARRASCO-ZEVALLOS O. M., KELLER B., VIEHLAND C., SHEN L., WATERMAN G., TODORICH B., SHIEH C., HAHN P., FARSIU S., KUO A. N., TOTH C. A., IZATT J. A.: Live volumetric (4D) visualization and guidance of in vivo human ophthalmic surgery with intraoperative optical coherence tomography. *Scientific Reports 6*, 1 (oct 2016), 31689. 1, 2

[CZVK*17] CARRASCO-ZEVALLOS O. M., VIEHLAND C., KELLER B., DRAELOS M., KUO A. N., TOTH C. A., IZATT J. A.: Review of intraoperative optical coherence tomography: technology and applications [Invited]. *Biomed. Opt. Express 8*, 3 (mar 2017), 1607–1637. 1

[DRN*17] DÍAZ J., ROPINSKI T., NAVAZO I., GOBBETTI E., VÁZQUEZ P. P.: An experimental study on the effects of shading in 3D perception of volumetric models. *Visual Computer 33*, 1 (2017), 47–61. 3

[EKP*17] EHLERS J. P., KHAN M., PETKOVSEK D., STIEGEL L., KAISER P. K., SINGH R. P., REESE J. L., SRIVASTAVA S. K.: Outcomes of Intraoperative OCT-Assisted Epiretinal Membrane Surgery from the PIONEER Study. *Ophthalmology Retina* (jul 2017). 1

[EUS18] EHLERS J. P., UCHIDA A., SRIVASTAVA S. K.: THE INTEGRATIVE SURGICAL THEATER: Combining Intraoperative Optical Coherence Tomography and 3D Digital Visualization for Vitreoretinal Surgery in the DISCOVER Study. *Retina 38* (sep 2018), S88–S96. 2

[KDK*19] KOLB J. P., DRAXINGER W., KLEE J., PFEIFFER T., EIBL M., KLEIN T., WIESER W., HUBER R.: Live video rate volumetric OCT imaging of the retina with multi-MHz A-scan rates. *PLOS ONE 14*, 3 (mar 2019), e0213144. 1, 2

[KW04] KRUGER J., WESTERMANN R.: Acceleration techniques for GPU-based volume rendering. *Proceedings of the 14th IEEE Visualization 2003 (VIS'03)* (2004), 287–292. 3

[REG18] ROIZENBLATT M., EDWARDS T., GEHLBACH P. L.: Robot-assisted vitreoretinal surgery: current perspectives. *Robotic Surgery: Research and Reviews Volume 5* (feb 2018), 1–11. 1

[RKH08] ROPINSKI T., KASTEN J., HINRICHS K. H.: Efficient shadows for GPU-based volume raycasting. *WSCG 2008* (2008), 17–24. 3

[SSN*98] SATO Y., SHIRAGA N., NAKAJIMA S., TAMURA S., KIKINIS R.: Local maximum intensity projection (LMIP): A new rendering method for vascular visualization. *J. Comput. Assist. Tomo. 22*, 6 (1998), 912–917. 2

[TT03] TKALCIC M., TASIC J.: Colour spaces: perceptual, historical and applicational background. In *The IEEE Region 8 EUROCON 2003. Computer as a Tool.* (2003), vol. 1, IEEE, pp. 304–308. 2

[VKCZ*16] VIEHLAND C., KELLER B., CARRASCO-ZEVALLOS O. M., NANKIVIL D., SHEN L., MANGALESH S., VIET DU T., KUO A. N., TOTH C. A., IZATT J. A.: Enhanced volumetric visualization for real time 4D intraoperative ophthalmic swept-source OCT. *Biomed Opt Express 7*, 5 (2016), 1815–1829. 2, 3, 4

[Zei] ZEISS AG: OPMI LUMERA 700 from ZEISS AG. URL: https://www.zeiss.com/meditec/int/product-portfolio/surgical-microscopes/ophthalmic-microscopes/opmi-lumera-700.html. 4

[ZEP11] ZHANG Q., EAGLESON R., PETERS T. M.: Volume Visualization: A Technical Overview with a Focus on Medical Applications. *Journal of Digital Imaging 24*, 4 (aug 2011), 640–664. 2